Development of the signal in sensory rhodopsin and its cognate transducer

ARTICLE *in* NATURE · APRIL 2006

Impact Factor: 41.46 · DOI: 10.1038/nature04520 · Source: PubMed

LETTERS

Development of the signal in sensory rhodopsin and its transfer to the cognate transducer

Rouslan Moukhametzianov[1,2]*, Johann P. Klare[3]*, Rouslan Efremov[1,2], Christian Baeken[1], Annika Göppner[3], Jörg Labahn[1], Martin Engelhard[3], Georg Büldt[1] & Valentin I. Gordeliy[1,2]

The microbial phototaxis receptor sensory rhodopsin II (NpSRII, also named phoborhodopsin) mediates the photophobic response of the haloarchaeon *Natronomonas pharaonis*[1,2] by modulating the swimming behaviour of the bacterium[3]. After excitation by blue-green light NpSRII triggers, by means of a tightly bound transducer protein (NpHtrII), a signal transduction chain homologous with the two-component system of eubacterial chemotaxis[4]. Two molecules of NpSRII and two molecules of NpHtrII form a 2:2 complex in membranes as shown by electron paramagnetic resonance[5] and X-ray structure analysis[6]. Here we present X-ray structures of the photocycle intermediates K and late M (M_2) explaining the evolution of the signal in the receptor after retinal isomerization and the transfer of the signal to the transducer in the complex. The formation of late M has been correlated with the formation of the signalling state[2,7]. The observed structural rearrangements allow us to propose the following mechanism for the light-induced activation of the signalling complex. On excitation by light, retinal isomerization leads in the K state to a rearrangement of a water cluster that partly disconnects two helices of the receptor. In the transition to late M the changes in the hydrogen bond network proceed further. Thus, in late M state an altered tertiary structure establishes the signalling state of the receptor. The transducer responds to the activation of the receptor by a clockwise rotation of about 15° of helix TM2 and a displacement of this helix by 0.9 Å at the cytoplasmic surface.

The initial event of signal transduction on excitation by light is the isomerization of the retinal chromophore from all-*trans* to 13-*cis*, followed by a series of spectroscopically and kinetically well characterized intermediate states[8,9]. The transition between M_1 and M_2 ($\tau = 2$ ms)[8] is thought to encompass the formation of the 'active' signalling state, which persists until the late intermediate O decays to the original ground state[2,7,10].

Crystals of NpSRII in complex with shortened transducer molecules (K state NpHtrII$_{1-114}$; M state NpHtrII$_{1-157}$) were grown in the lipidic cubic phase[11,12]. The ground-state structure of NpSRII in the complex (Fig. 1a) is almost identical to the structure of NpSRII alone[13,14]. The crystals of the complex were illuminated to freeze-trap the K and M intermediates. Single-crystal spectrophotometry was used to determine the amount of trapped intermediates (Fig. 1b). Because the M state is split into M_1 and M_2, which cannot be distinguished by their absorption spectra[15], we used flash-photolysis experiments (Fig. 1c), revealing 5% M_1 state and 49% M_2 state (Supplementary Methods). In the K state structural changes with respect to the ground state are observed within a sphere of 9 Å diameter around the central water cluster on the extracellular side of the retinal (Fig. 2a). The isomerization of the retinal bound to Lys 205 gives rise to a displacement of its Cε and Cδ atoms by 1.1 Å, whereas the backbone atoms show almost no changes from the ground state. This shift reduces the distance between Lys 205-Cε and the ground-state position of water molecule 1 (W1-O) from 3.3 to 2.5 Å. Therefore the pentagonal structure of hydrogen bonds including water molecules W1 to W3 and the oxygen atoms of the aspartic residues Asp 75 and Asp 201 found for the ground state can no longer exist in the K state. W1 is sterically driven away from its original location; presumably it shows positional disorder in a cavity formed by the retinal, Asp 75 and Thr 79.

The charge separation between the protonated Schiff-base nitrogen and Asp 75-Oδ increases from 4.2 Å to 4.9 Å in the K state. As observed for the K state of the receptor alone[16], the carboxylic group of Asp 75 in the complex is rotated by about 90° from its ground-state conformation, thereby losing the hydrogen bond to Thr 79. Consequently W3 becomes disordered. The hydrogen bond structure (Asp 201-Oδ···W2···W4···Arg 72-Nε) is retained, although W2 and W4 shift towards the retinal by about 1.5 Å in the K state. The distance from Asp 201-Oδ to the Schiff-base nitrogen is reduced from 4.9 Å to 2.7 Å as a result of the movement of the Schiff base. The conformation of Arg 72 is not affected by the cascade of changes launched by the photoisomerization of retinal. For all observed photocycle states this residue shows a conformation corresponding to that of Arg 82 in the bacteriorhodopsin M state (Fig. 2c), where it is part of the proton release chain[17,18].

During the transition from K state to M_1 state the proton of the Schiff base translocates to Asp 75 (refs 19, 20). Because there is a distance of almost 5 Å in the K state between the Schiff-base nitrogen and Asp 75, the thermal mobility of these groups may be of crucial importance for the proton transfer to succeed. Indeed, during the reaction path from the ground state through K to late M the temperature factor of Asp 75-Oδ2 varies from 18 Å^2 (B_G) through 31 Å^2 (B_K) to 22 Å^2 (B_M) and the distance between Asp 75-Oδ2 and the Schiff-base nitrogen relaxes from 4.9 Å in the K state to 4.3 Å in late M (Fig. 2b), when proton transfer has occurred.

In late M state a further hydrogen bond connecting helices C and G in the K state through water molecules W2′ and W4′ has vanished (Figs 2b and 3a). Consequently these helices now have more freedom to move independently (Fig. 3; see also stereo view in Supplementary Fig. S1). Difference densities clearly show changes in the position of the main chain that are not present in the K state (for example Arg 72; Fig. 2b). The helical segment between Pro 71 and Pro 81 in helix C is displaced towards the central water cluster by 0.4 Å with respect to the ground state, although the centre of mass of helix C is moving slightly outwards. Water molecule W2′ shifts towards Asp 75 and Arg 72 (Fig. 2b).

The main structural changes in late M state are displacements of

[1]Research Centre Jülich, Institute of Structural Biology (IBI-2), 52425 Jülich, Germany. [2]Centre for Biophysics and Physical Chemistry of Supramolecular Structure, MIPT, 141700 Dolgoprudny, Russia. [3]Max Planck Institute for Molecular Physiology, Otto Hahn Strasse 11, 44227 Dortmund, Germany.
*These authors contributed equally to this work.

helices (Fig. 3) that appear after the loss of interhelical connections between helices C and G in the central water cluster (Fig. 2b). Furthermore, the movement of a proton from the Schiff base to Asp 75 alters the charge distribution in this region so that the resulting electrostatic interactions might also influence the tertiary structure. To obtain an overview of all changes in the tertiary structure of the complex we have calculated a double-distance matrix of the difference of the Cα atom distances in late M minus the corresponding distances in the ground state (Supplementary Figure S2). This matrix reveals that the receptor is divided into two domains with respect to the relative motions of the helices. The relative motion of helix A with respect to helices B and G is quite small, so these helices are part of the domain ABG. The other domain consists of helices C, D, E and F because double distances between these helices are also quite small (Supplementary Figure S2). Helices in each of the domains are connected by van der Waals contacts along their complete length including several intercalating bulky aromatic side chains. Furthermore, there are several hydrogen bonds between side chains as well as interhelical connections involving water molecules contributing to the rigidity within the domains. The relative movement of these two domains requires structural changes at the interaction surfaces of helices B–C (not shown) and helices F–G (Figs 3b, c and 4a). These interfaces are formed almost exclusively by leucine and isoleucine residues, which allow relative movements (shear motions) of helices by moderate changes of side-chain torsion angles of about 10°. The neighbouring helices B and C of the two domains exert only small movements with respect to each other, whereas helices F and G, the other pair of interdomain helices, have larger relative movements in the direction to membrane normal. Figure 3b, c and 4 show that the main part of this movement is a shift of helix G towards the extracellular side in late M with respect to helix F. Obviously domain ABG is nearly fixed at the interface between helices B and C and the ABG domain moves with the shift observed at the interface between helices F and G. The relative displacement of helices F and G is stabilized in late M state by the formation of a hydrogen bond between Asp 214 and Arg 162, which might contribute to the longer M_2-state and O-state lifetimes than those of bacteriorhodopsin. It should be noted that the behaviour of helix F is different from that observed for the late M state of bacteriorhodopsin, in which helix F exerted an outward bending motion[18,21,22], and also that deduced from electron paramagnetic resonance (EPR)[5,10] and biochemical[23] studies for NpSRII. This could have two causes: the larger EF loop of bacteriorhodopsin compared with the short loop in NpSRII and/or packing interactions with the adjacent layers in the crystal. The outward movement of helix F in bacteriorhodopsin opens the cytoplasmic domain for the penetration of water molecules, which are necessary for the reprotonation of the Schiff base and Asp 96. In contrast to this, NpSRII, when complexed with its transducer, is not pumping protons[24,25], so an opening of the cytoplasmic domain is not required.

Apart from a possible contribution of electrostatic interactions to the signal transfer, which are also effective over larger distances, the signal transfer by short-range interactions takes place in the interface between helices F, G and TM2. All hydrogen bonds between receptor and transducer observed for the ground state are still intact in late M state (Fig. 4a). Our X-ray structures show a constant hydrogen-bond length of 2.6 Å between Tyr 199 (helix G) and Asn 74 (helix TM2) and a parallel shift of both amino acids by about 0.6 Å to the extracellular side in late M. Changes in distance between helix F and TM2 are quite small with the exception of the cytoplasmic side, where a distance

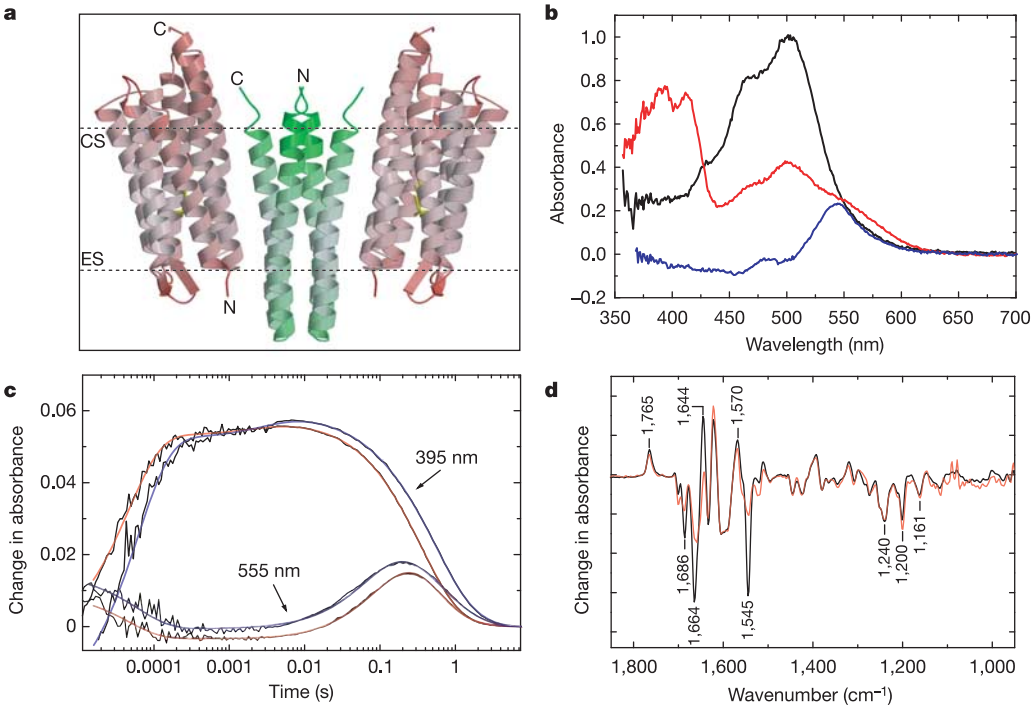

Figure 1 | Crystal structure of the complex and its spectroscopic characterization. a, Crystal structure of the complex in the ground state consisting of two molecules of NpSRII (red) with two molecules of NpHtrII (green). The ribbon diagram of the side view of the complex in *B*-factor colouring: light red and green indicate less mobile; dark red and green indicate mobile. ES, extracellular side; CS, cytoplasmic side. The dotted lines confine the hydrophobic core of the protein. **b**, Low-temperature (100 K) absorbance spectrum of the complex in crystals: ground state (black), trapped M state (red) and a difference spectrum of trapped K state minus ground state (blue). **c**, Photocycle kinetics of the complex in crystals and of the complex reconstituted in polar lipids from purple membranes of *Halobacterium salinarum* in 3 M sodium phosphate pH 5.6 at 25 °C. Traces of transient absorbance difference of the complex at 390 and 555 nm show the time evolution of the M and O states. Raw data are shown in black, and exponential fits are shown in red and blue for the complex in liposomes and in crystals, respectively. **d**, Difference FTIR spectra of illuminated minus non-illuminated complex in the crystal (red) and reconstituted in liposomes (black) measured at room temperature.

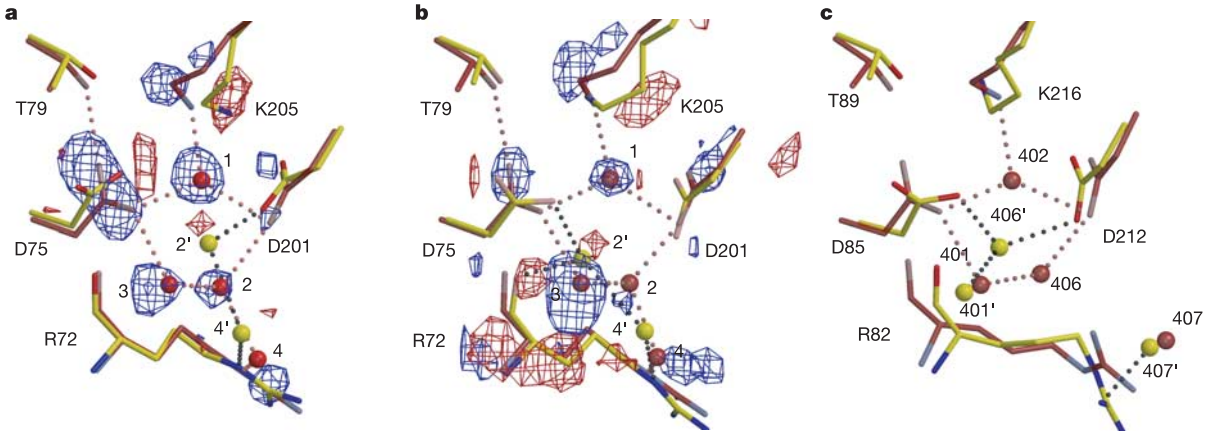

Figure 2 | Structural changes in the extracellular vicinity of the retinal Schiff base. Hydrogen-bond pattern including four water molecules, Lys 205, Asp 75, Asp 201, Arg 72 and Thr 79 side chains, showing ground state (red), intermediate states (yellow), water molecules of ground state (red balls) and intermediate states (yellow balls). Hydrogen bonds are shown as red dotted lines for the ground state and as black dotted lines for the intermediate states. Difference densities are shown in blue for negative densities and red for positive densities (Methods). **a**, K state of complex with electron density maps contoured at 4.5σ and -4.5σ. **b**, M intermediate of complex with electron density maps contoured at 3σ and -3σ. **c**, Analogue residues of ground-state and late M-state structures of bacteriorhodopsin (Protein Data Bank accession code 1CWQ).

increase of 0.6 Å is observed (Fig. 4b, Supplementary Figure S2), for an in-plane movement of TM2. Double distances of helix G and TM2 are larger, so that helix G has an active function in changing the interaction surface faced by TM2 and in this way conducts the signal from the receptor to the transducer. Figures 3c and 4 show that the signal transfer produces a clockwise rotation of TM2 by 15° (observed from the cytoplasmic side) and a tilt of TM2 giving an in-plane displacement of 0.9 Å at the cytoplasmic side with the hinge at Gly 66 near Ser 62, which is hydrogen-bonded to Thr 189 (helix G). A rotation of TM2 has already been deduced by EPR experiments of site-directed spin-labelled transducer and receptor molecules[5]. It is striking that the transfer of the signal from the receptor to the transducer is accompanied by an amplification, as reflected by larger amplitudes (rotation and displacements) in the transducer than in the receptor.

Fourier-transform infrared (FTIR) experiments on the complex show a decreased intensity in amide I and II bands in crystals compared with that in liposomes (Fig. 1d), although the localization of bands is conserved, indicating smaller conformational changes in crystals. It may be that the layer packing within the crystal, predominantly observed between EF and BC loops, restrains the motion of helix F in late M, as mentioned above, or that there are differences in the structure of the region of residues 83–157 that could not be traced.

Thus, light-activated signal transfer from receptor to transducer originates in the isomerization of retinal, which induces local changes in the hydrogen-bonding network in a region near the retinal (K state). During the transition to the signalling state (late M) these disturbances increase so that in late M fewer hydrogen bonds connect helices C and G. These alterations in the hydrogen-bond network change the pK_a values of the Schiff base and the proton acceptor group Asp 75, thereby enabling proton transfer, which produces a redistribution of charges. Both causes give rise to changes in the tertiary structure of the receptor in late M. Signal transfer to the transducer takes place within the interface of receptor helices F and G and transducer helix TM2. The main effect on TM2 is a clockwise rotation of about 15° and a tilt of the helix, with the hinge at Ser 62, that amounts to 0.9 Å at the cytoplasmic side (Leu 77). The cytoplasmic end of TM2 rolls over the surface from helix F to G, whereas the extracellular side of TM2 remains fixed. There is a

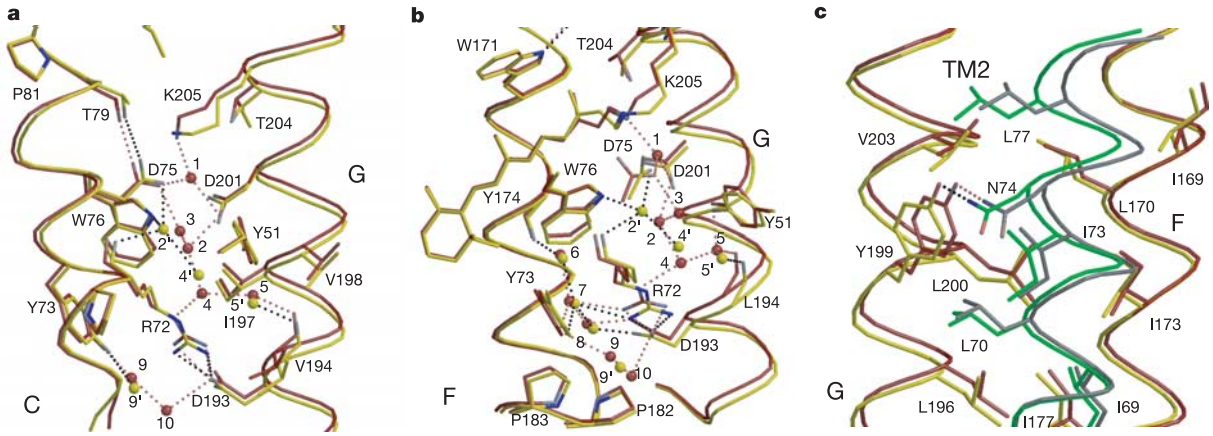

Figure 3 | Interhelical interactions. Changes in helical structure and interactions between ground state (red) and late M state (yellow) including water molecules as red and yellow balls; the hydrogen-bonded network is shown in red for the ground state and in black for late M state. **a**, Helices C and G; **b**, helices F and G; **c**, helixes F, G and TM2 (transducer helix in grey for ground state and in green for late M state).

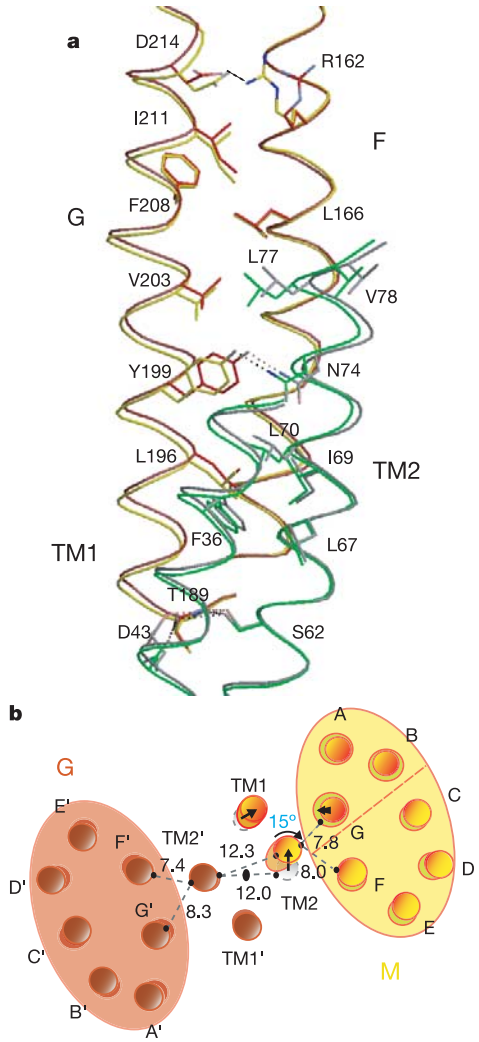

Figure 4 | Overall views of helices F, G, TM1 and TM2 in ground and late M states. a, Structural changes along these helices; colours are as in Fig. 3c. **b**, Schematic picture of helical displacements viewed from the cytoplasmic surface. The ground-state complex is shown in red and the late M-state complex in yellow; black numbers give distances between Cα atoms of the following amino acids in the ground and late M states: F(Leu 170) to TM2(Leu 77), ground state 7.4 Å, M state 8.0 Å; G(Val 203) to TM2(Leu 77), ground state 8.3 Å, M state 7.8 Å; TM2(Val 78) to TM2′(Val 78), ground state 12.0 Å, M state 12.3 Å. The arrows on TM1 and TM2 depict displacements parallel to the membrane plane in late M; the thick arrow on helix G depicts its 0.5 Å movement to the extracellular side. A clockwise rotation of 15° is observed for TM2 and an in-plane displacement of 0.9 Å (black arrow) near the cytoplasmic membrane surface in late M state with respect to the ground state. A red line in the receptor coloured yellow divides the molecule into the two functionally important domains ABG and CDEF. The inner red shaded circles of helices A, B and G depict their movements to the extracellular side.

combination of rotation and tilt; the latter appears as an in-plane displacement of the cytoplasmic end of TM2.

METHODS

Protein preparation and crystallization. Protein preparation and crystallization were performed as described previously[5,6].

Trapping of intermediates. To obtain the highest yield in the occupancy of the K and M states we always used the optimum wavelength and intensity of an argon ion laser. The K state was accumulated by illumination of the crystal at 100 K for 20 s with the argon laser (472 nm, about 10 mW mm^{-2}). For trapping late M state the crystal was left to warm up to about 20 °C (by blocking the nitrogen cryostream), illuminated for 3 s with argon laser light at 488 nm (about 30 mW mm^{-2}), then cooled (by unblocking the cryostream) while the blue light was still on. One second after recooling started, the illumination was turned off. X-ray data were collected in darkness.

Spectroscopic characterization of the crystals. Visual and FTIR spectra of single crystals (Fig. 1b–d) were measured with an infrared microscope described elsewhere[12]. Visual absorption spectra (Fig. 1b) were recorded from single crystals in the nitrogen cryostream under conditions identical to those used for X-ray measurements.

Treatment of diffraction data. X-ray diffraction data (wavelength 0.934 Å) were collected at beamlines ID14-1 and ID13 of the European Synchrotron Radiation Facility (ESRF), Grenoble, France. Low-resolution and high-resolution data sets (1° oscillation) were obtained from several crystals (for ground state seven crystals were used; for K state three were used; for late M state five were used). Diffraction pattern were processed with MOSFLM/SCALA (CCP4). To compare the quality of the different data sets a range of R_{merge} was determined by calculating R_{merge} between pairs of data sets (ground state, 0.07–0.09; K state, 0.10–0.12; M state, 0.15–0.17; ground with M state, 0.22–0.25). The first three values show that the difference in diffraction for each state is in a narrow range whereas the fourth value shows the overall change between the ground and M states. Crystallographic parameters and refinement statistics are summarized in Supplementary Table 1 for two of the best crystals, one crystal for the K state and one larger crystal for the ground and M states using different spots for the same crystal. The mean $[I/\sigma I]$ value for the ground state is smaller than for the M state, as a result of the weak reflections at the high-resolution shells. When calculating mean $[I/\sigma I]$ for the ground state at the M-state resolution of 2.2 (2.26–2.2) Å, values of 8.0 (5.6) were obtained. In our refinement, doubtful reflections were rejected with the strong criterion $F/\sigma F < 2$, resulting in a smaller number of reflections used in the refinement (Supplementary Table 1).

Refinement. Starting from a polyalanine model of NpSRII/NpHtrII(1–114) (Protein Data Bank accession code 1H2S; ref. 6) the molecular replacement (MOLREP) solution was completed by the automated refinement procedure (ARP)[26] using ground state data. Residues 23–82 of the transducer were built. Simulated annealing and individual *B*-factor refinement were used (CNS)[27]. Several data sets from non-illuminated crystals gave almost identical models of the ground state with a mean coordinate variation of 0.1 Å, which fits with σ_A values in the K and late M states of 0.16 and 0.12 Å, respectively.

Difference density maps $\Delta\rho = (|F_{ill}| - |F_{Gobs}|)\exp(i\phi_G)$ revealed major structural changes that occurred on illumination of the crystals (Fig. 2a, b), with $|F_{ill}|$ being the observed amplitudes from illuminated crystals, $|F_{Gobs}|$ the observed ground-state amplitudes and ϕ_G the phases calculated from the ground-state model. Refinements of intermediate states were performed by starting with a superposition of a fixed and a refinable ground-state structure with occupancies varying in the range 0.2–0.8 by simulating annealing (using 3,000 and 5,000 K and a slow cooling protocol in CNS). Extrapolated densities were calculated for refined models $\rho_{ex} = (1-\alpha)|F_G|[\exp(i\phi_G)] + \alpha|F_X|[\exp(i\phi_X)]$ with different occupancies α for the intermediate state and correlated with observed omit densities $\rho_{omit} = |F_{ill}|[\exp(i\phi_{Gomit})]$, with $|F_G|$ being the amplitudes of the ground-state model, $|F_X|$ and ϕ_X being the amplitudes and phases of the intermediate-state models for the K state or late M state, and ϕ_{Gomit} being the phases calculated from the ground-state model where atoms are omitted. Intermediate state occupancies were estimated from the best correlation as 40 ± 10% for the K state and 50 ± 10% for late M state. This variation had no significant effect on the conformation for the intermediate state after refinement. After occupancy had been fixed, models were further refined and manually rebuilt in program O until convergence of *R* factors was reached. The significance of structural changes was also proven by Supplementary Fig. S3.

Spectroscopic analysis of crystals trapped in the K state contained about 50% K state and 50% ground state so that a refinement by two models for ground and K states is justified. Crystals trapped in the M_2 state contained small amounts of the O, M_1 and K states. The quantity in the M_1 state was estimated to be about 5% and that in the K state even lower. A refinement of crystals trapped in late M by a ground-state and M_2-state model is therefore justified because traces of intermediates less than 10% cannot be detected at our resolution.

Received 25 October; accepted 15 December 2005.
Published online 1 February 2006.

1. Spudich, J. L. Variations on a molecular switch—transport and sensory signalling by archaeal rhodopsins. *Mol. Microbiol.* **28**, 1051–1058 (1998).
2. Klare, J. P. *et al.* The archaeal sensory rhodopsin II/transducer complex: a model for transmembrane signal transfer. *FEBS Lett.* **564**, 219–224 (2004).

3. Scharf, B. E. & Wolff, E. K. Phototactic behaviour of the archaebacterial *Natronobacterium pharaonis*. *FEBS Lett.* **340,** 114–116 (1994).
4. Rudolph, J. & Oesterhelt, D. Deletion analysis of the *che* operon in the archaeon *Halobacterium salinarium*. *J. Mol. Biol.* **258,** 548–554 (1996).
5. Wegener, A. A., Klare, J. P., Engelhard, M. & Steinhoff, H.-J. Structural insights into the early steps of receptor–transducer signal transfer in archaeal phototaxis. *EMBO J.* **20,** 5312–5319 (2001).
6. Gordeliy, V. I. *et al.* Molecular basis of transmembrane signalling by sensory rhodopsin II–transducer complex. *Nature* **419,** 484–487 (2002).
7. Yan, B., Takahashi, T., Johnson, R. & Spudich, J. L. Identification of signaling states of a sensory receptor by modulation of lifetimes of stimulus-induced conformations: The case of sensory rhodopsin II. *Biochemistry* **30,** 10686–10692 (1991).
8. Chizhov, I. *et al.* The photophobic receptor from *Natronobacterium pharaonis*: Temperature and pH dependencies of the photocycle of sensory rhodopsin II. *Biophys. J.* **75,** 999–1009 (1998).
9. Hirayama, J. *et al.* Photocycle of phoborhodopsin from haloalkaphilic bacterium (*Natronobacterium pharaonis*) studied by low-temperature spectrophotometry. *Biochemistry* **31,** 2093–2098 (1992).
10. Wegener, A. A., Chizhov, I., Engelhard, M. & Steinhoff, H.-J. Time-resolved detection of transient movement of helix F in spin-labelled *Pharaonis* sensory rhodopsin II. *J. Mol. Biol.* **301,** 881–891 (2000).
11. Landau, E. M. & Rosenbusch, J. P. Lipidic cubic phases: A novel concept for the crystallization of membrane proteins. *Proc. Natl Acad. Sci. USA* **93,** 14532–14535 (1996).
12. Gordeliy, V. I., Schlesinger, R., Efremov, R., Büldt, G. & Heberle, J. in *Membrane Protein Protocols: Expression, Purification, and Crystallization* (ed. Selinsky, B.) 305–316 (Humana Press, Totowa, New Jersey, 2003).
13. Royant, A. *et al.* X-ray structure of sensory rhodopsin II at 2.1-Å resolution. *Proc. Natl Acad. Sci. USA* **98,** 10131–10136 (2001).
14. Luecke, H. *et al.* Crystal structure of sensory rhodopsin II at 2.4 angstroms: Insights into colour tuning and transducer interaction. *Science* **293,** 1499–1503 (2001).
15. Balashov, S. P., Sumi, M. & Kamo, N. The M intermediate of *Pharaonis* phoborhodopsin is photoactive. *Biophys. J.* **78,** 3150–3159 (2000).
16. Edman, K. *et al.* Early structural rearrangements in the photocycle of an integral membrane sensory receptor. *Structure* **10,** 473–482 (2002).
17. Luecke, H., Richter, H.-T. & Lanyi, J. K. Proton transfer pathways in bacteriorhodopsin at 2.3 angstrom resolution. *Science* **280,** 1934–1937 (1998).
18. Sass, H. J. *et al.* Structural alterations for proton translocation in the M state of wild-type bacteriorhodopsin. *Nature* **406,** 649–653 (2000).
19. Engelhard, M., Scharf, B. E. & Siebert, F. Protonation changes during the photocycle of sensory rhodopsin II from *Natronobacterium pharaonis*. *FEBS Lett.* **395,** 195–198 (1996).
20. Furutani, Y., Iwamoto, M., Shimono, K., Kamo, N. & Kandori, H. FTIR Spectroscopy of the M photointermediate in pharaonis phoborhodopsin. *Biophys. J.* **83,** 3482–3489 (2002).
21. Koch, M. H. *et al.* Time-resolved X-ray diffraction study of structural changes associated with the photocycle of bacteriorhodopsin. *EMBO J.* **10,** 521–526 (1991).
22. Subramaniam, S., Gerstein, M., Oesterhelt, D. & Henderson, R. Electron diffraction analysis of structural changes in the photocycle of bacteriorhodopsin. *EMBO J.* **12,** 1–8 (1993).
23. Yoshida, H., Sudo, Y., Shimono, K., Iwamoto, M. & Kamo, N. Transient movement of helix F revealed by photo-induced inactivation by reaction of a bulky SH-reagent to cysteine-introduced pharaonis phoborhodopsin (sensory rhodopsin II). *Photochem. Photobiol. Sci.* **3,** 537–542 (2004).
24. Bergo, V. B., Spudich, E. N., Rothschild, K. J. & Spudich, J. L. Photoactivation perturbs the membrane-embedded contacts between sensory rhodopsin II and its transducer. *J. Biol. Chem.* **280,** 28365–28369 (2005).
25. Schmies, G., Engelhard, M., Wood, P. G., Nagel, G. & Bamberg, E. Electrophysiological characterization of specific interactions between bacterial sensory rhodopsins and their transducers. *Proc. Natl Acad. Sci. USA* **98,** 1555–1559 (2001).
26. Perrakis, A. *et al.* Automated protein model building combined with iterative structure refinement. *Nature Struct. Biol.* **6,** 458–463 (1999).
27. Brunger, A. T. *et al.* Crystallography and NMR system: a new software suite for macromolecular structure determination. *Acta Crystallogr. D* **54,** 905–921 (1998).

Supplementary Information is linked to the online version of the paper at www.nature.com/nature.

Acknowledgements We thank K.-E. Jaeger and H. Gieren for their help in expressing NpSRII; G. Kachalova, J. Granzin and J. Heberle for scientific discussions; B. Gehrmann for administrative assistance; the staff of beamlines ID14-1 and ID13, in particular E. Mitchell; and the staff of beamline X13 at DESY, in particular W. R. Rypniewski. This study was supported by the Deutsche Forschungsgemeinschaft, the Max-Planck-Gesellschaft, the Alexander von Humboldt Foundation and the Helmholtz Association of National Research Centres.

Author Information The coordinates for these structures have been deposited in the Protein Data Bank under accession codes 2F93 and 2F95. Reprints and permissions information is available at npg.nature.com/reprintsandpermissions. The authors declare no competing financial interests. Correspondence and requests for materials should be addressed to G.B. (g.bueldt@fz-juelich.de) or M.E. (martin.engelhard@mpi-dortmund.mpg.de).